Supporting Information

Spatial decoupling strategy boosted alkaline hydrogen evolution for efficient solar-driven AEM electrolyzer

*Minghui Cui [a], Yansong Zhou [a], Rongjing Guo [b], Wenqi Zhao [a], Yanjing Liu [a], Qiongrong Ou [a, *], Shuyu Zhang [a, *]*

[a] State Key Laboratory of Photovoltaic Science and Technology, Institute for Electric Light Sources, School of Information Science and Technology, Fudan University, Shanghai, 200433, China.

[b] Texas Materials Institute and Department of Mechanical Engineering, The University of Texas at Austin, Austin, Texas, 78712, United States.

* Corresponding authors.

E-mail addresses: qrou@fudan.edu.cn (Q. Ou), zhangshuyu@fudan.edu.cn (S. Zhang).

Material Characterizations

The morphologies of the samples were conducted by scanning electron microscope (SEM, thermo scientific Apreo 2C) and transmission electron microscopy (TEM, FEI Talos F200S). X-ray diffraction (XRD) patterns were recorded on a Rigaku Ultima IV X-ray diffractometer using Cu-Kα source, with a scan step of $2°$ min^{-1}. X-ray photoelectron spectroscopy (XPS) analyses were recorded on a ThermoFischer ESCALAB Xi+ XPS instrument at a pressure of $8×10^{-10}$ Pa using Al Kα X-ray, carbon calibration at 284.8 eV. The consumption of Pt in the electrolyte after deposition was measured using a plasma mass spectrometer (ICP-OES, PE Avio 200) to obtain the loading of Pt.

Electrochemical Characterizations

The electrochemical tests were performed on an electrochemical workstation (CHI 760E, Shanghai Chenhua, China), using a three-electrode system. The prepared samples were used as working electrodes directly, while saturated Hg/HgO electrode and high-purity graphite rod were used as reference electrode and counter electrode, respectively. The measured potential against the reference electrode was converted to a reversible hydrogen electrode (RHE) by the following formula E(RHE)=E(Hg/HgO)+0.098+0.059×pH. The linear sweep voltammetry (LSV) polarization curves were recorded in the range of 0.1 to -1 V (vs. RHE) with a scan rate of 5 mV s^{-1}. The polarization curves were calibrated with 90% iR compensation. The electrochemically active surface area (ECSA) of samples was obtained by measuring the cyclic voltammetry (CV) curves from 0.1~0.2 V (vs. RHE) with different scan rates (10~50 mV s^{-1}). ECSA can be calculated by equation ECSA= C_{dl}/C_s, where Cs is the specific capacitance of the sample which is usually 0.040 mF cm^{-2} in the alkaline solution. Electrochemical impedance spectroscopy (EIS) was performed in the

frequency range from 10^5 to 0.01 Hz with an amplitude of 5 mV at an overpotential of 100 mV. The long-term stability was determined by testing the chronopotentiometry (v-t) curve at a current density of 500 mA cm^{-2}.

Theoretical calculations

All calculations were performed using CP2K [1]. The Gaussian Plane Waves (GPW) method in the QUICKSTEP module was utilized with the double-zeta valence polarized DZVP-MOLOPT-SR-GTH basis set [2] and the norm-conserving GTH-PBE pseudopotential. [3] Three-dimensional periodic boundary conditions were applied, incorporating approximately a 20 Å vacuum layer in the Z direction. A cut-off energy of 500 Ry was used for the planewave expansion, and each Gaussian was mapped onto a 60 Ry cut-off grid. Dispersion was accounted for using D3(BJ) [4, 5] in all calculations. The electron distribution was characterized using the Fermi-Dirac function at an electronic temperature of 300 K. The convergence threshold for the density matrix during the self-consistent field process was set at 10^{-7} Ry. The default setting was used as the convergence limit for geometric optimization.

In the thermodynamic calculation, Gibbs free energy change is determined by enthalpy change, zero-point energy correction (ZPE) and entropy of the system, as shown in the following formula:

$$\Delta G_{H^*} = \Delta E_{H^*} + \Delta_{ZPE} - T\Delta S$$

Where ΔE_{H^*} is the chemisorption energy of hydrogen atom, is equivalent to the thermal correction of the internal energy at 0 K which measures the difference between the adsorbed state and the gas phase. The third term is related to the entropy of the system and can be calculated from the partition function. Considering the simplicity of practical calculation, some approximations can be used to get the result:[6]
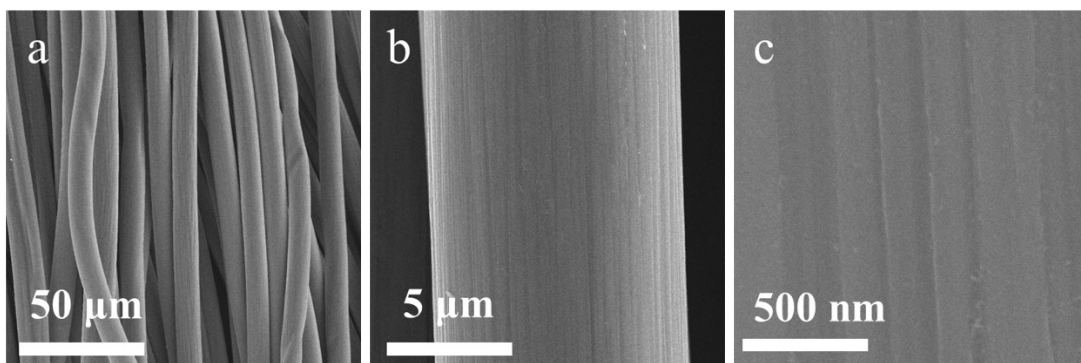
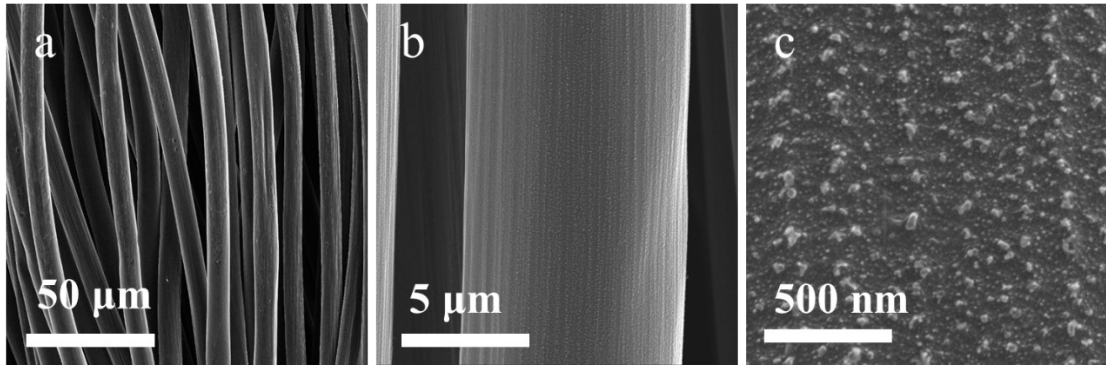$$\Delta G_{H^*} = \Delta E_{H^*} + 0.24(eV)$$

a

b

c

d
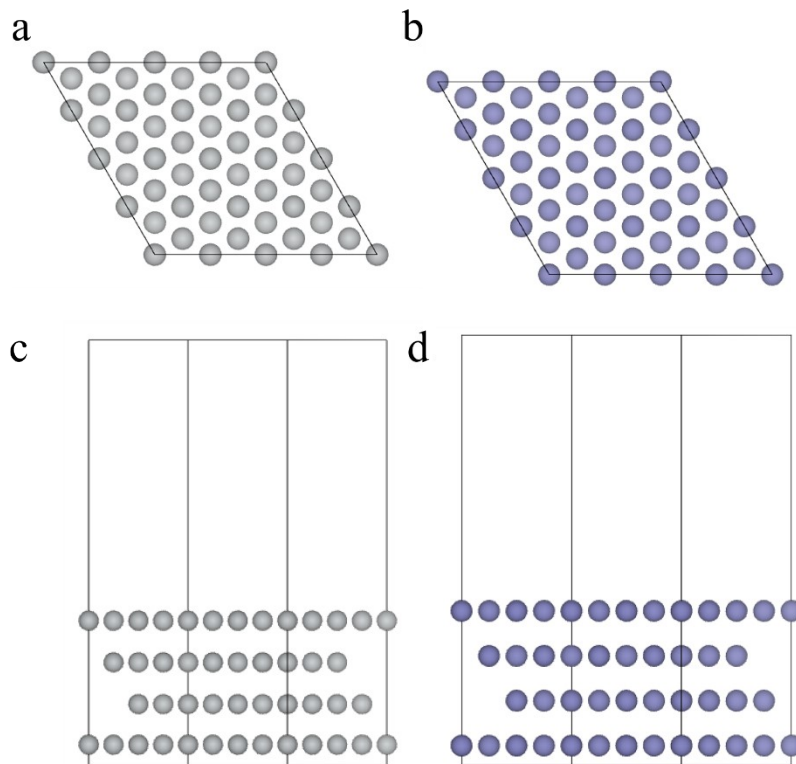
Fig. S1. Top and side view of the atomic structure models of (a, c) Ni (111) and (b, d)
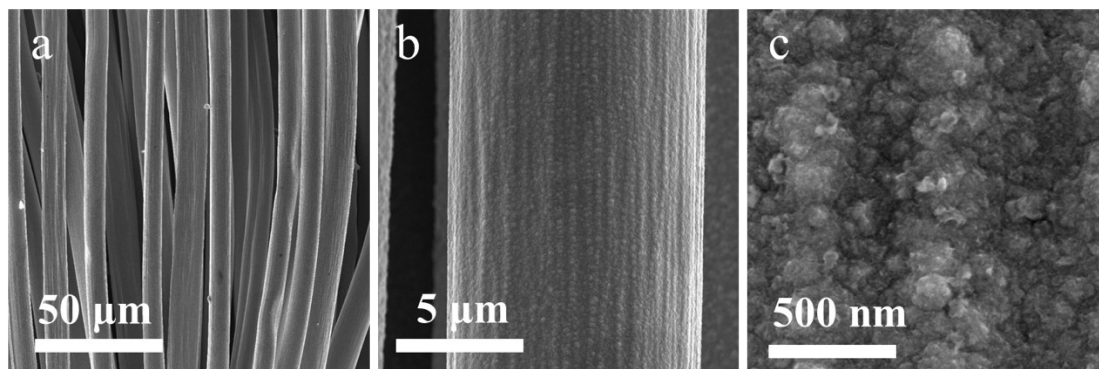
Pt (111).
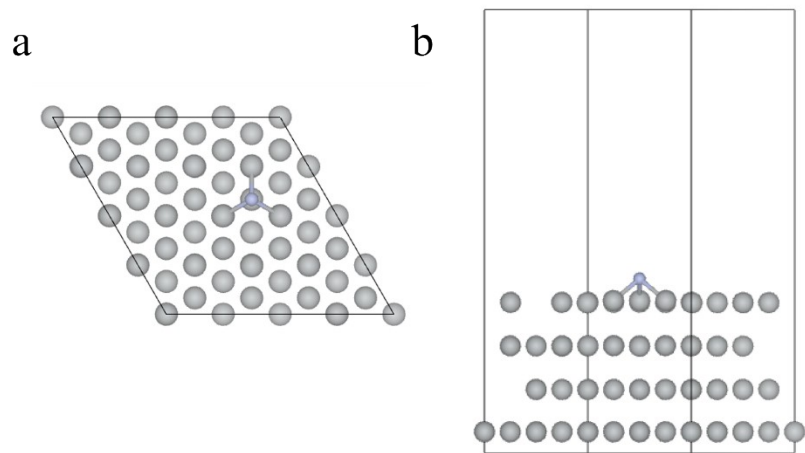
Fig. S2. (a) Top and (b) side view of the atomic structure models of N-Ni.

Fig. S3. SEM images of CC
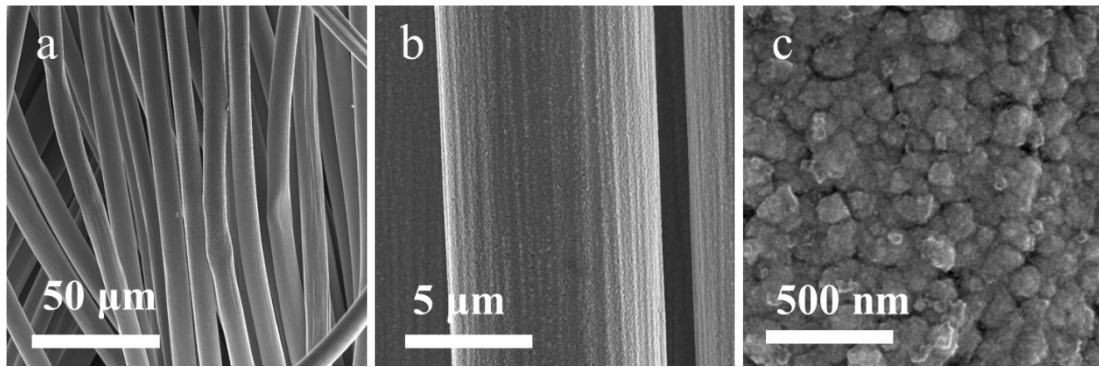
Fig. S4. SEM images of NC.

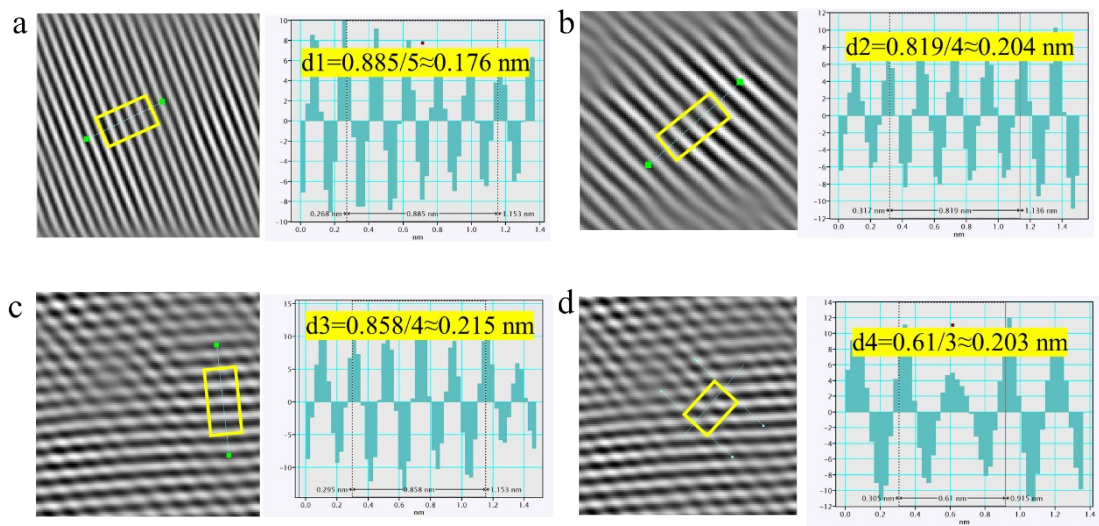**Fig. S5.** SEM images of Ni/NC.

Fig. S6. SEM images of N-Ni/NC.

Fig. S7. Interplanar spacing measurement of d1~d4 in Fig. 2b.
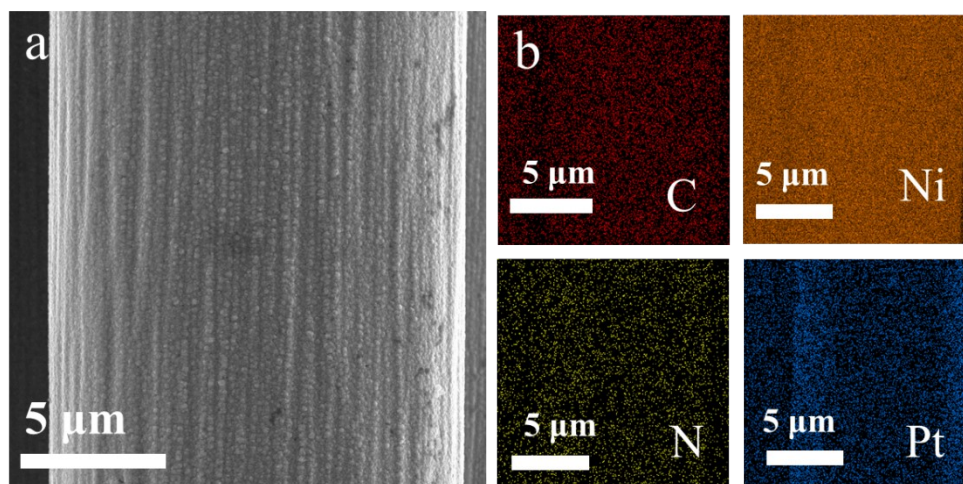
Fig. S8. (a) SEM image and (b) EDS element mapping of Pt-N-Ni/NC.
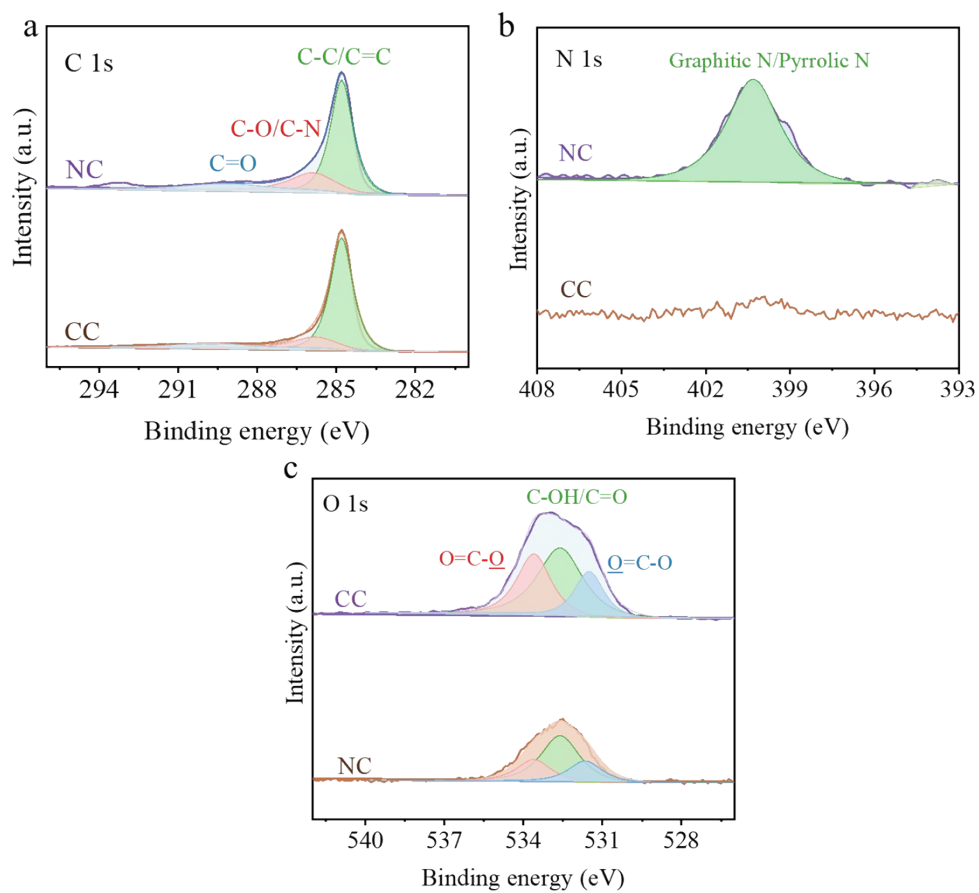
Fig. S9. (a) C 1s, (b) N 1s and (c) O 1s high resolution XPS spectrums of CC and NC.
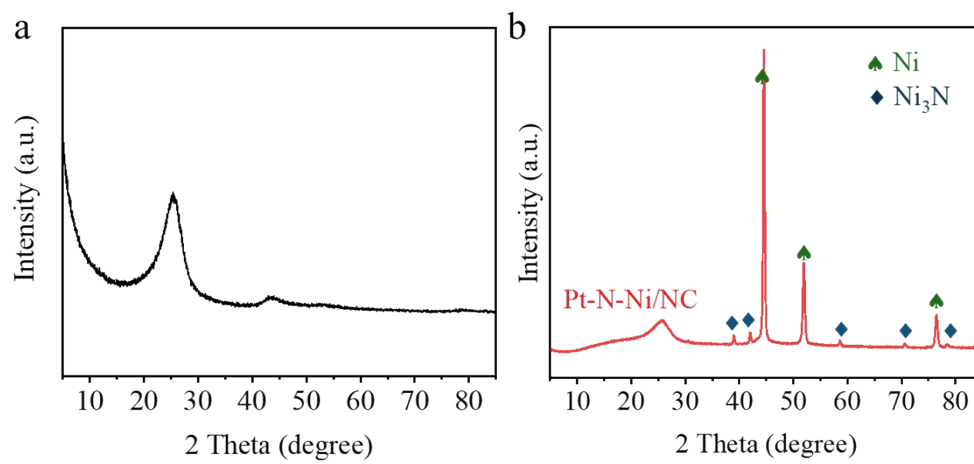
Fig. S10. XRD patterns of (a) CC and (b) Pt-N-Ni/NC.
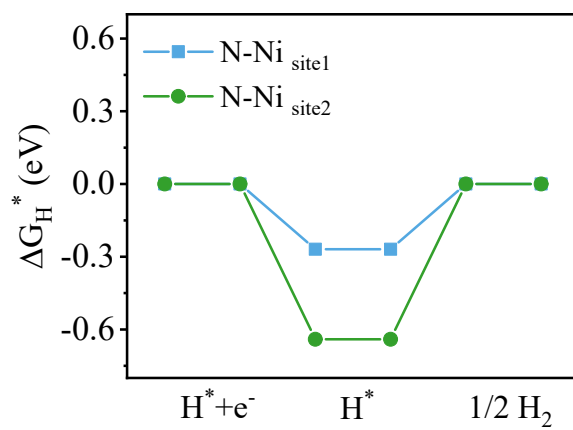
Fig. S11. ΔG_{H*} on the surface of N-Ni.
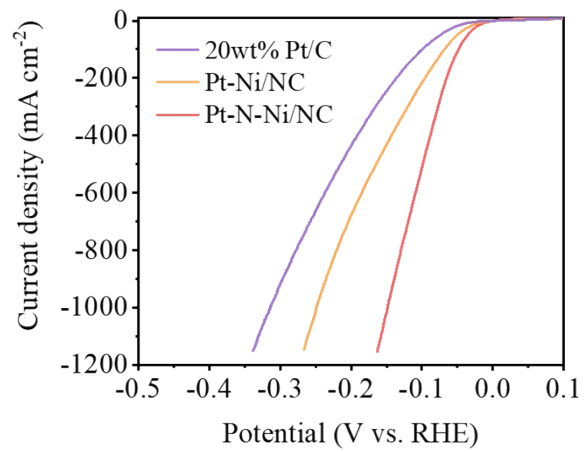
Fig. S12. Polarization curves of 20 wt% Pt/C, Pt-Ni/NC and Pt-N-Ni/NC.
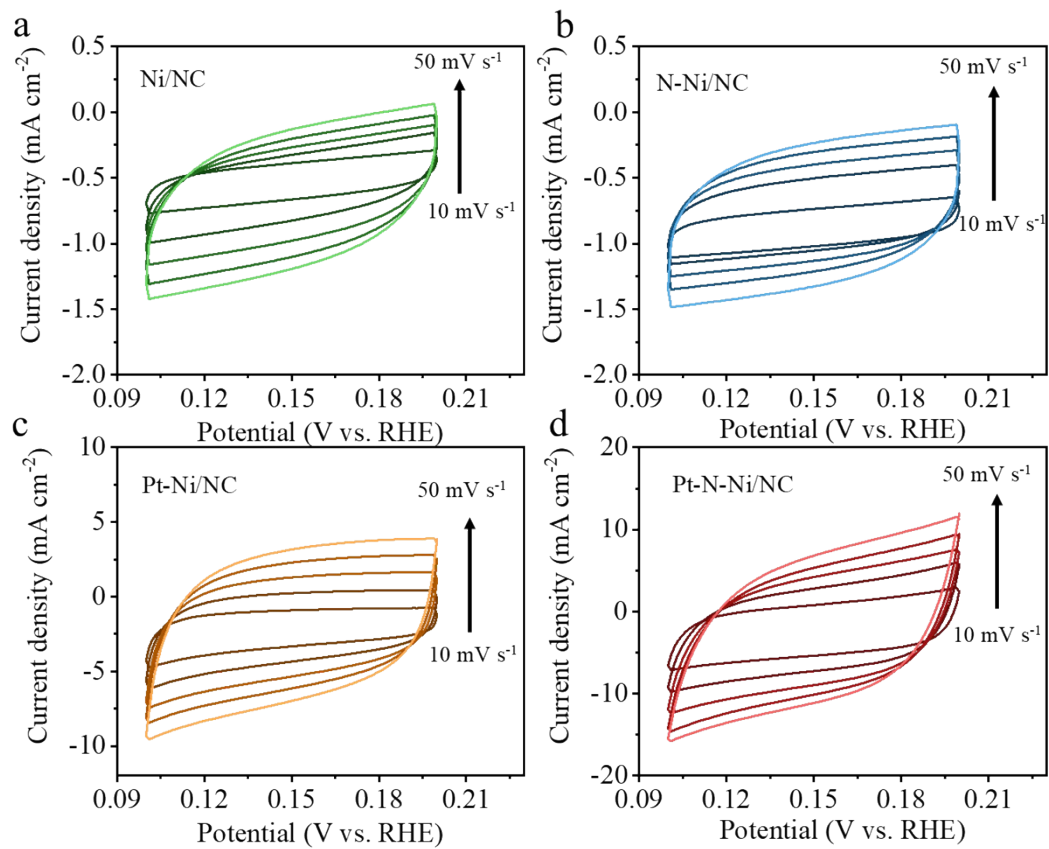
Fig. S13. CV measurement of (a) Ni/NC, (b) N-Ni/NC, (c) Pt-Ni/NC and (d) Pt-N-Ni/NC with scan rates of 10~50 mV s^{-1}.
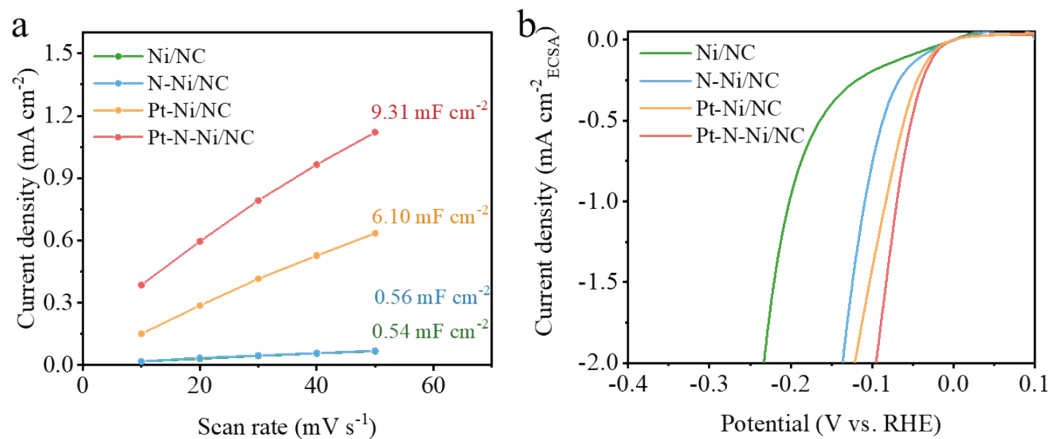
Fig. S14. Capacitive current as a function of scan rate (half of the slope is C_{dl}). (b) Polarization curves from Fig. 3a normalized to the ECSA.
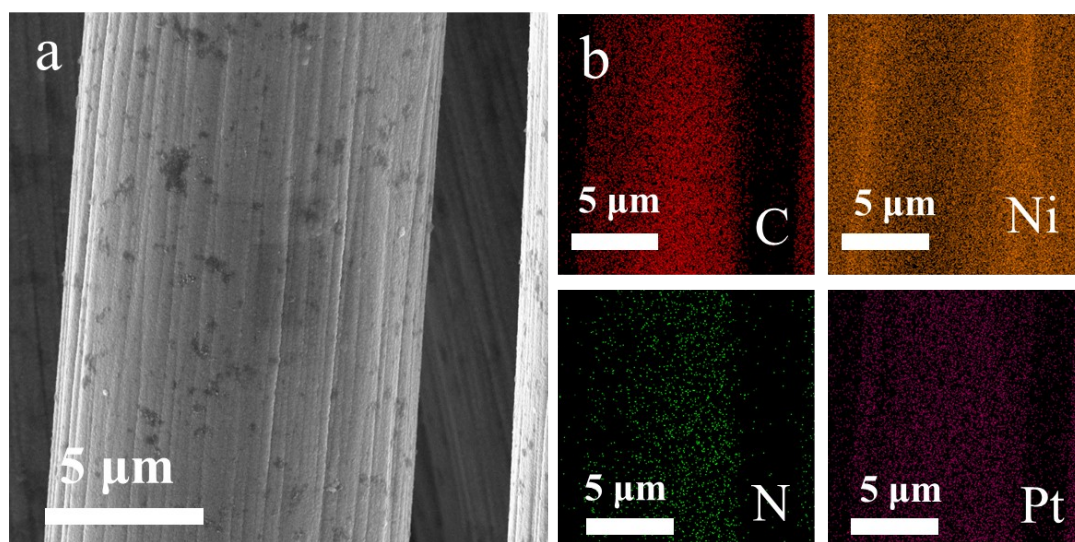
Fig. S15. (a) SEM image and (b) EDS element mapping of Pt-N-Ni/NC after long-term stability testing.
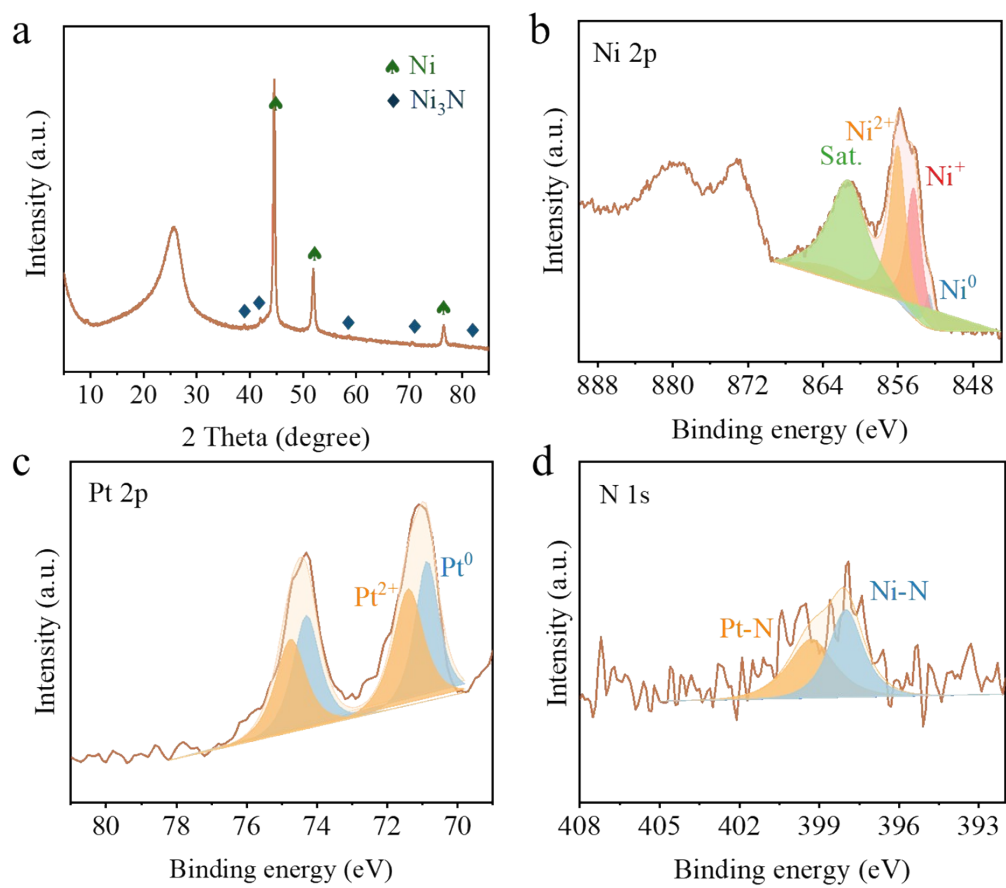
Fig. S16. (a) XRD pattern, (b) Ni 2p, (c) Pt 2p and (d) N 1s high resolution XPS spectrum of Pt-N-Ni/NC after long-term test.

Table S1. Parameters of commercial solar cell.

Active material	Pm(W)	Isc(A)	Voc(V)	Ipm(A)	Vpm(V)	FF
Si	22.75	7.59	3.98	7.14	3.19	0.75

Pm: maximum power, Isc: short-circuit current, Voc: open-circuit voltage, Ipm: current at maximum power point, Vpm: voltage at maximum power point, FF: filling factor.

Table S2. The HER catalytic activity compared with other reported literatures.

Catalyst	Current density (mA cm^{-2})	Overpotential (mV)	Tafel slop (mV dec^{-1})	Ref.
Pt-N-Ni/NC	10	15	44.9	This work
	1000	149		
Pt/GaN	10	24	48.9	[7]
	1000	441		
Pt/TiO$_2$/Ni(OH)$_2$	10	26	38.9	[8]
	1000	145		
Pt/D-NiFe LDH	10	28	43	[9]
	1000	217		
Ru-CoO$_x$/NF	10	20	28	[10]
	1000	252		
Pt/8-NCNT	10	17	33.3	[11]
	1000	153		
np/Pt$_1$Ru$_1$-Ni$_{0.85}$Se	10	46	32.4	[12]
	1000	225		
Pt$_2$/Ni(OH)$_2$/NF	10	19	70	[13]
	1000	274		
NA-Ru$_3$Ni/C	10	14	28	[14]
	1000	168		
Pt-NiMo-OH/NF	10	34	30.5	[15]
	1000	221		
Fe-PtNiPO	10	19	35	[16]
	1000	193		
Ru-Ni(OH)$_2$	10	15	37	[17]
	1000	267		

Table S3. Comparison of catalyst performance in AEM electrolyzers with other literatures.

Cathode	Anode	Anion exchange membrane	Current density $(A\ cm^{-2})$	Voltage (V)	Ref.
Pt-N-Ni/NC	NiFeOOH	PiperION A-40	0.5	1.63	This work
			1	1.75	
Raney nickel	$NiFe_2O_4$	Sustainion X37-50 Grade T	1	1.83	[18]
NiMoN/NF	d-(Fe,Ni)OOH/NF	Sustainion X37-50 Grade RT	0.5	1.795	[19]
Ni_3N/Ni/Ti mesh	$NiFe_2O_4$/SS fiber	Fumapem FAA-3-50	0.5	1.88	[20]
Pt/C	Ni_2P/Ni_7S_6	Fumasep FAA-3–50	1	1.88	[21]
r-Ru-Ni/NiO	NiFe LDH	Fumasep FAA-3–50	1	2.03	[22]
20% Pt/C	Mo-CoOOH/NF	HoAM Grion 1204	1	2.02	[23]
Pt@–NiFe LDH	S–NiFe LDH	Fumasep FAA-3-PK-130	0.5	2.5	[24]
NiFeCo phosphide	NiFeCo LDH	Sustainion X37-50 Grade RT	0.5	1.72	[25]
Co_2P–$Ni_{12}P_5$/NF	Fe_2P–$Ni_{12}P_5$/NF	Fumasep FAA-3–50	1	1.95	[26]
Pt mesh	Ni_2P/FeP_2/MN	FAA-3-50	1	1.88	[27]
Pt-AC/Cr–N–C	NiFe LDH	Sustainion X37-50	0.5	1.78	[28]
			1	1.9	

Table S4. Comparison of solar-driven water splitting with other literatures.

Cathode	Anode	Current density (mA cm^{-2})	STH (%)	Ref.
Pt-N-Ni/NC	FeNiOOH	1390	8.33	This work
Pt/C	NiFeCo-OOH	571	12.44	[29]
nickel nanomesh	nickel nanomesh	≈60	9.98	[30]
Pt/C/CPF	Ni-TFBDC/CFP	206.7	10.17	[31]
Co-OSP	Co-OSP	≈8	9.80	[32]
NiMoP/NF	NiFeP/NF	11.6	14.30	[33]
Ce-NiMo-PS@NF	Ce-NiMo-PS@NF	16.5	18.69	[34]
PCO-nHI	PCO-nHI	9.9	11.50	[35]
CoP/CTF	CoP/CTF	10.5	16.80	[36]
Co$_2$P-MoNiP/NF	NiFe-LDH/NF	16	19.68	[37]
CoP@Ni$_2$P-Fe$_2$P	CoP@Ni$_2$P-Fe$_2$P	12.46	15.33	[38]
S-FeNiOOH	S-FeNiOOH	6	7.20	[39]
Pt–Ti	a-NiFeOOH/N-CFP	161	8.14	[40]

References

1. T. D. Kühne, M. Iannuzzi, M. Del Ben, V. V. Rybkin, P. Seewald, F. Stein, T. Laino, R. Z. Khaliullin, O. Schütt and F. Schiffmann, *J. Chem. Phys.*, 2020, **152**.

2. J. VandeVondele and J. Hutter, *J. Chem. Phys.*, 2007, **127**.

3. M. Krack, *Theor. Chem. Acc.*, 2005, **114**, 145-152.

4. S. Grimme, J. Antony, S. Ehrlich and H. Krieg, *J. Chem. Phys.*, 2010, **132**.

5. S. Grimme, S. Ehrlich and L. Goerigk, *J. Comput. Chem.*, 2011, **32**, 1456-1465.

6. J. K. Nørskov, T. Bligaard, A. Logadottir, J. Kitchin, J. G. Chen, S. Pandelov and U. Stimming, *J. Electrochem. Soc.*, 2005, **152**, J23.

7. C. Liu, C. Niu, B. Gao, P. Jiang, Q. Lin, W. Wu, Y. Jia, Z. Wei and Q. Xu, *ChemNanoMat*, 2023, **9**, e202300195.

8. A. Kong, M. Peng, M. Liu, Y. Lv, H. Zhang, Y. Gao, J. Liu, Y. Fu, W. Li and J. Zhang, *Appl. Catal. B*, 2022, **316**, 121654.

9. Z. Wu, Z. Chen, K. Xu, B. Li, Z. Li, G. Xu, W. Xiao, T. Ma, Y. Fu and L. Wang, *Renewable Energy*, 2023, **210**, 196-202.

10. D. Wu, D. Chen, J. Zhu and S. Mu, *Small*, 2021, **17**, 2102777.

11. W. Yu, H. Huang, Y. Qin, D. Zhang, Y. Zhang, K. Liu, Y. Zhang, J. Lai and L. Wang, *Adv. Energy Mater.*, 2022, **12**, 2200110.

12. L. Cai, H. Bai, C.-w. Kao, K. Jiang, H. Pan, Y.-R. Lu and Y. Tan, *Small*, 2024, **n/a**, 2311178.

13. J. Sun, Z. Zhang and X. Meng, *Appl. Catal. B*, 2023, **331**, 122703.

14. L. Gao, F. Bao, X. Tan, M. Li, Z. Shen, X. Chen, Z. Tang, W. Lai, Y. Lu, P. Huang, C. Ma, S. C. Smith, Z. Ye, Z. Hu and H. Huang, *Energy Environ. Sci.*, 2023, **16**, 285-294.

15. X. Zhang, Y. Han, W. Cai, D. Zhang, Z. Wang, H. Li, Y. Sun, Y. Zhang, J. Lai and L. Wang, *Adv. Mater. Interfaces*, 2022, **9**, 2102154.

16. K. Feng, J. Xu, Y. Chen, S. Li, Z. Kang and J. Zhong, *Adv. Sci.*, 2022, **9**, 2203199.

17. Y. Zhang, Z. Li, L. Hou and X. Liu, *Adv. Funct. Mater.*, 2023, **33**, 2213976.

18. B. Motealleh, Z. Liu, R. I. Masel, J. P. Sculley, Z. Richard Ni and L. Meroueh, *Int. J. Hydrogen Energy*, 2021, **46**, 3379-3386.

19. L. Wu, M. Ning, X. Xing, Y. Wang, F. Zhang, G. Gao, S. Song, D. Wang, C. Yuan, L. Yu, J. Bao, S. Chen and Z. Ren, *Adv. Mater.*, 2023, **35**, 2306097.

20. D. Zhang, H. Li, A. Riaz, A. Sharma, W. Liang, Y. Wang, H. Chen, K. Vora, D. Yan, Z. Su, A. Tricoli, C. Zhao, F. J. Beck, K. Reuter, K. Catchpole and S. Karuturi, *Energy Environ. Sci.*, 2022, **15**, 185-195.

21. F.-L. Wang, N. Xu, C.-J. Yu, J.-Y. Xie, B. Dong, X.-Y. Zhang, Y.-W. Dong, Y.-L. Zhou and Y.-M. Chai, *Appl. Catal. B*, 2023, **330**, 122633.

22. N. Xu, J.-Y. Lv, H.-Y. Sun, X.-J. Tian, W.-L. Yu, X. Li, C.-Y. Liu, Y.-M. Chai and B. Dong, *J. Colloid Interface Sci.*, 2024, **664**, 704-715.

23. L. Tang, L. Yu, C. Ma, Y. Song, Y. Tu, Y. Zhang, X. Bo and D. Deng, *J. Mater. Chem. A*, 2022, **10**, 6242-6250.

24. H. Lei, Q. Wan, S. Tan, Z. Wang and W. Mai, *Adv. Mater.*, 2023, **35**, 2208209.

25. J. Lee, H. Jung, Y. S. Park, N. Kwon, S. Woo, N. C. S. Selvam, G. S. Han, H. S. Jung, P. J. Yoo, S. M. Choi, J. W. Han and B. Lim, *Appl. Catal. B*, 2021, **294**, 120246.

26. L. Guo, X. Liu, Z. He, Z. Chen, Z. Zhang, L. Pan, Z.-F. Huang, X. Zhang, Y. Fang and J.-J. Zou, *ACS Sustain. Chem. Eng.*, 2022, **10**, 9956-9968.

27. J. Xie, F. Wang, Y. Zhou, Y. Dong, Y. Chai and B. Dong, *Nanomicro Lett*, 2023,

16, 39.

28.   A. Kong, M. Peng, M. Liu, Y. Lv, H. Zhang, Y. Gao, J. Liu, Y. Fu, W. Li and J. Zhang, *Appl. Catal. B*, 2022, **316**, 121654.

29.   J. S. Ha, Y. Park, J.-Y. Jeong, S. H. Lee, S. J. Lee, I. T. Kim, S. H. Park, H. Jin, S. M. Kim, S. Choi, C. Kim, S. M. Choi, B. K. Kang, H. M. Lee and Y. S. Park, *Adv. Sci.*, 2024, **n/a**, 2401782.

30.   N. Plankensteiner, A. Agosti, J. Govaerts, R. Rupp, S. Singh, J. Poortmans, P. M. Vereecken and J. John, *Solar RRL*, 2023, **7**, 2201095.

31.   X. Li, X. Wu, B. Li, S. Zhang, Y. Liu, Z. Li, D. Zhang, X. Wang, Q. Sun, D. Gao, C. Zhang, W.-H. Huang, C.-C. Chueh, C.-L. Chen, S. Yang, S. Xiao, Z. Wang and Z. Zhu, *ACS Nano*, 2023, **17**, 23478-23487.

32.   B. Chong, M. Xia, Y. Lv, H. Li, X. Yan, B. Lin and G. Yang, *Chem. Eng. J.*, 2023, **465**, 142853.

33.   H. Roh, H. Jung, H. Choi, J. W. Han, T. Park, S. Kim and K. Yong, *Appl. Catal. B*, 2021, **297**, 120434.

34.   Y. Cheng, A. Yuan, Y. Zhang, H. Liu, J. Du and L. Chen, *J. Colloid Interface Sci.*, 2024, **660**, 166-176.

35.   G. Y. Jang, S. Kim, J. Choi, J. Park, S. An, J. Baek, Y. Li, T.-K. Liu, E. Kim, J. H. Lee, H. Wang, M. Kim, H.-S. Cho, X. Zheng, J. S. Yoo, K. Seo and J. H. Park, *Adv. Energy Mater.*, 2024, **14**, 2303924.

36.   S. Min, Z. Meng, Y. Zhao, W. Li, Z. Zhang and F. Wang, *Sustainable Energy & Fuels*, 2024, **8**, 310-321.

37.   Y. Zhao, H. Zhang, J. Chen, S. Zhao, M. Xi, L. Yang, Y. Long, Z. Ni, Y. Zhou and A. Chen, *Chem. Eng. J.*, 2023, **477**, 147092.

38.   K. Chang, D. T. Tran, J. Wang, K. Dong, S. Prabhakaran, D. H. Kim, N. H. Kim

and J. H. Lee, *Appl. Catal. B*, 2023, **338**, 123016.

39.   C. Kim, S. H. Kim, S. Lee, I. Kwon, S. H. Kim, S. Kim, C. Seok, Y. S. Park and

Y. Kim, *J. Energy Chem.*, 2022, **64**, 364-371.

40.   P. Thangavel, G. Kim and K. S. Kim, *J. Mater. Chem. A*, 2021, **9**, 14043-14051.